materials

MDPI

Article

Investigation on Preparation and Performance of High Ga CIGS Absorbers and Their Solar Cells

Xiaoyu Lv [1], Zilong Zheng [1], Ming Zhao [2], Hanpeng Wang [2] and Daming Zhuang [2,*]

[1] Faculty of Materials and Manufacturing, Beijing University of Technology, Beijing 100124, China; lxy4518@emails.bjut.edu.cn (X.L.); zilong.zheng@bjut.edu.cn (Z.Z.)
[2] School of Materials Science and Engineering, Tsinghua University, Beijing 100084, China; zhaoming2013@tsinghua.edu.cn (M.Z.); wanghp20@mails.tsinghua.edu.cn (H.W.)
* Correspondence: dmzhuang@tsinghua.edu.cn

Abstract: Tandem solar cells usually use a wide band gap absorber for top cell. The band gap of $CuIn_{(1-x)}Ga_xSe_2$ can be changed from 1.04 eV to 1.68 eV with the ratio of Ga/(In+Ga) from 0 to 1. When the ratio of Ga/(In+Ga) is over 0.7, the band gap of CIGS absorber is over 1.48 eV. CIGS absorber with a high Ga content is a possible candidate one for the top cell. In this work, CuInGa precursors were prepared by magnetron sputtering with CuIn and CuGa targets, and CIGS absorbers were prepared by selenization annealing. The Ga/(In+Ga) is changed by changing the thickness of CuIn and CuGa layers. Additionally, CIGS solar cells were prepared using CdS buffer layer. The effects of Ga content on CIGS thin film and CIGS solar cell were studied. The band gap was measured by PL and EQE. The results show that using structure of CuIn/CuGa precursors can make the band gap of CIGS present a gradient band gap, which can obtain a high open circuit voltage and high short circuit current of the device. With the decrease in Ga content, the efficiency of the solar cell increases gradually. Additionally, the highest efficiency of the CIGS solar cells is 11.58% when the ratio of Ga/(In+Ga) is 0.72. The value of Voc is 702 mV. CIGS with high Ga content shows a great potential for the top cell of the tandem solar cell.

Keywords: CIGS; Ga content; CuIn/CuGa precursors; tandem solar cell; band gap energy

check for updates

Citation: Lv, X.; Zheng, Z.; Zhao, M.; Wang, H.; Zhuang, D. Investigation on Preparation and Performance of High Ga CIGS Absorbers and Their Solar Cells. *Materials* **2023**, *16*, 2806. https://doi.org/10.3390/ma16072806

Academic Editors: Vilko Mandić, Luka Pavic, Ivana Capan and Ivana Panžić

Received: 9 March 2023
Revised: 26 March 2023
Accepted: 28 March 2023
Published: 31 March 2023

Copyright: © 2023 by the authors. Licensee MDPI, Basel, Switzerland. This article is an open access article distributed under the terms and conditions of the Creative Commons Attribution (CC BY) license (https://creativecommons.org/licenses/by/4.0/).

1. Introduction

As environmental issues become increasingly serious, people focus on the decomposition of pollutants [1–3] and the use of clean energy [4–6]. Photovoltaic materials can convert solar energy into electric energy, which can make full use of solar energy. Chalcopyrite phase $CuIn_{(1-x)}Ga_xSe_2$ (CIGS) based solar cell has been the focus of research due to its high absorption coefficient and adjustable band gap and high potential efficiency. With the increase in Ga content, the band gap of CIGS varies from 1.04 eV to 1.67 eV [7]. The highest efficiency of CIGS solar cells obtained with the ratio of Ga/(In+Ga) (GGI) of 0.30 is 23.35% [8]. Thus, great efforts have been made for high efficiency as a single p-n junction CIGS solar cell almost with GGI of 0.2 to 0.3. There are few studies on CIGS with high GGI. Nowadays, tandem solar cells have attracted considerable attention [9–11]. Thus, CIGS with high Ga content is considered to be a suitable material for top cells of CIGS based tandem solar cells due to its high band gap [12–15]. M. Schmid et al. prepared simply stacked $CuGaSe_2/Cu(In,Ga)Se_2$ tandem cell and achieved a efficiency of 8.5% [16]. The efficiency of CGS top cell is only 4.3%. They thought that the top cell performs an important role in the tandem solar cell. Hedayati M et al. obtained 32.3% efficiency cell by using CGS/CIGS tandem solar cells through simulation, and the top cell used is CGS solar cell with 16% efficiency [17]. Thus, a top cell with high quality is necessary for tandem solar cells. Additionally, CIGS with high GGI is a promising candidate for the top cells in tandem systems.

In the multi-compounds system, the system of the similar bonding and varying stoichiometry can be assessed by systematic atomistic modeling, which can explain the variation of their specific properties [18]. In the $CuInGaSe_2$ system, the band gap varies with the different ratio of Ga/(In+Ga). Through the hybrid density functional theory study, the conduction band of CIGS consists by In, Ga, and Se s orbitals. With the increasing of GGI, the density of the states from In s orbitals becomes lower, thus, the band gap of CIGS increases [19]. With the increase in Ga content, the band gap of CIGS solar cells can be calculated by [20]

$$E_g(eV) = 1.04 + 0.63x - 0.21x(1 - x) \quad (1)$$

where x is the Ga/(In+Ga) ratio. Samira Khelif et al. calculated that the optimal band gap range of the top cell of the top cell is 1.5–1.7 eV [21]. For CIGS with Ga content from 0.7 to 1.0, the band gap can be changed between 1.45 eV to 1.67 eV. With the increase in the band gap, a higher open circuit voltage (Voc) can be obtained. However, the short circuit current (Jsc) would decrease because of the lower absorption limit. Therefore, the double-graded band gap of CIGS absorbers can enhance their photovoltaic performance [22,23]. A high band gap at the surface results in a high Voc. Meanwhile, a lower band gap minimum can improve the Jsc of the absorber.

CIGS solar cells with high Ga content are mainly prepared by evaporation [24,25], electrodeposition [26] and molecular beam epitaxy [27], and magnetron sputtering and selenide post-treatment [28,29]. Among these preparations, magnetron sputtering and selenide post-treatment processes are considered to have the advantage of large area uniformity [30]. However, CIGS films fabricated by sputtering CIGS quaternary have small grains, which may limit the efficiency of the solar cells [31,32]. Therefore, using CuGa and CuIn target sputtering, and selenide post-treatment is used to prepare CIGS solar cells. The precursor prepared with CuGa and CuIn alloy targets were annealed in a selenium-containing atmosphere, which can make the grains grow fully [33]. Additionally, the ratio of GGI can be adjusted easily.

In this work, CuInGa precursors were prepared by magnetron sputtering with CuIn and CuGa targets, and CIGS absorbers were prepared by selenization annealing, and the physical properties of CIGS films were investigated. At the same time, CIGS solar cells were prepared, and the effects of different Ga content on the performance of solar cells were investigated as well.

2. Materials and Methods

The structure of CIGS solar cell fabricated in this work was SLG/Mo/CIGS/CdS/i-ZnO/AZO. CuIn and CuGa precursors were deposited on Mo-coated soda-lime glass (SLG) substrates by middle-frequency magnetron sputtering from $Cu_{0.8}In$ and $Cu_{0.8}Ga$ alloy targets. First, 800 nm Mo was prepared on SLG by magnetron sputtering. In order to make the precursor uniform, we used a target with a larger size of 360 × 80 × 6 mm, the sputtering background pressure was 2×10^{-3} Pa, the sputtering gas was Ar, and the pressure was 0.7 Pa. Using CuIn/CuGa as the precursor, the CuIn layer was below the CuGa layer. The content of Ga in the precursor was changed by changing the sputtering thickness of CuIn and CuGa precursors. The designed values of GGI were 0.7, 0.8, 0.9, and 1.0, respectively. The total thickness of the precursor was designed as 500 nm. The prepared precursor subjected to selenization annealing in a vacuum annealing furnace. In order to stabilize and fully conduct the reaction, two steps of temperature rise were used for annealing. The base pressure of the annealing furnace was 2×10^{-3} Pa. The temperature of the first step is 450 °C, last for 30 min; The temperature of the second stage is 540 °C, last for 40 min. The mixture of hydrogen selenide and argon was used for selenization, and the concentration of hydrogen selenide was 3%. The thickness of the CIGS films was about 1 μm. The CdS buffer layer was prepared by the CBD method. The i-ZnO and AZO window layers were prepared by magnetron sputtering, with thickness of 80 nm and 600 nm, respectively.

The inductively coupled plasma optical emission spectrometer (ICP-OES, IRIS Intrepid II, Thermo Fisher Scientific, Waltham, MA, USA) was used to measure Ga concentration in CIGS films. The morphologies of CIGS thin films were observed by SEM (Merlin VP Compact, Zeiss, Jena, Germany). The phase structures were characterized by X-ray diffraction (XRD, D/max-2550, Rigaku, Tokyo, Japan). The surface band gap was measured by PL, the 532 nm laser line was used for photoluminescence (PL) excitation. The device performance parameters of CIGS cells were characterized by a Volt-Ampere characteristic tester (2400, Keithley, Cleveland, OH, USA) and a solar simulator (91,192–1000, Newport, Oxfordshire, UK) under AM 1.5G illumination at 25 °C. The external quantum efficiency spectra of CIGS preparation solar cells were measured by a QETest Station 2000ADI system (Crowntech, Hong Kong).

3. Results

3.1. Results and Discussion

3.1.1. $Cu(In,Ga)Se_2$ Growth and Characterization

Table 1 shows the specific components of CIGS absorption layer with different Ga contents. The contents of Cu, In, Ga, and Se were obtained by ICP, Ga/(In+Ga) are 1.00, 0.90, 0.81, and 0.72, respectively. Figure 1 shows SEM images of the surface and cross-sectional morphologies of CIGS films with Ga/(In+Ga) ratio of 1.00, 0.90, 0.81, and 0.72, respectively, on Mo-coated SLG substrate.

Table 1. Elemental compositions of the CIGS films.

Sample	Cu (at%)	In (at%)	Ga (at%)	Se (at%)	Ga/(In+Ga)
A	22.8	0	25.1	52.1	1.00
B	22.6	2.4	22.7	52.3	0.90
C	22.6	4.8	20.5	52.1	0.81
D	22.4	6.9	18.2	52.5	0.72

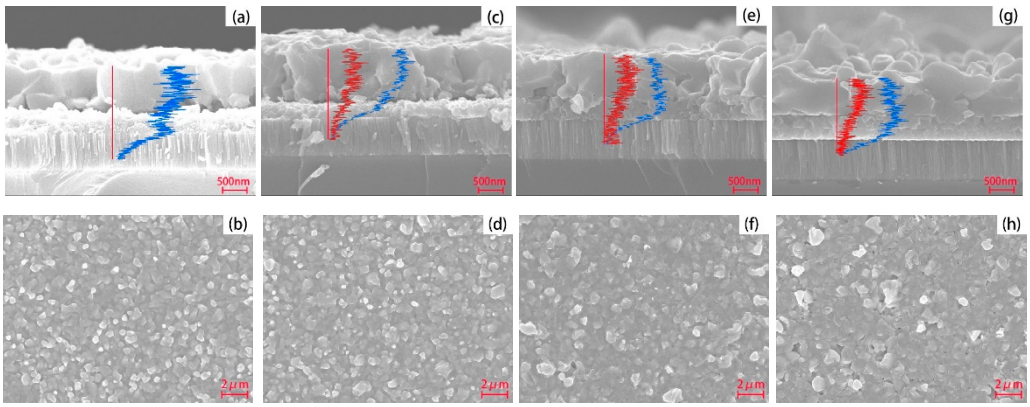

Figure 1. Cross-sectional and surface SEM images: (**a**,**b**) for GGI = 1.00; (**c**,**d**) for GGI = 0.90; (**e**,**f**) for GGI = 0.81; (**g**,**h**) for GGI = 0.72. The red line is for the distribution of indium along the depth of the CIGS film, the blue line is for the distribution of selenium along the depth of the CIGS film.

According to the surface images, all samples show good crystallinity and grains are closely arranged. With the increase in indium content, holes begin to appear on the surface of the absorption layer and, at the same time, the planeness of the surface decreases. This is because of the structure of the precursor. CuIn layer was deposited at the bottom half and CuGa layer was deposited at the upper half. In the H_2Se atmosphere, indium showed more effective than gallium, resulting in the decrease in the flatness [34,35]. The blue line is for the distribution of selenium along the depth of the CIGS film. In the samples with GGI of 1.00 and 0.90, the content of Se near Mo layer decreases significantly, forming a layer with high Ga content. This is because the reaction rate of Cu-Se combination is higher than

that of Ga-Se, which makes Ga aggregate near Mo layer, resulting in a layer with high Ga content that is difficult to selenide at Mo/CIGS surface. The red line is for the distribution of indium along the depth of the CIGS film. With the increase in indium content, the combination reaction between Cu-In-Ga-Se is more likely to occur, reducing the tendency of enrichment of Ga toward Mo. When Ga content is 0.81, Se can be evenly distributed in the CIGS film. For Sample B, Sample C, and Sample D, the distribution of indium is increased first, at the depth of about 300 nm, indium content reaches the maximum value. It means that at the depth of 300 nm, the CIGS film has a minimum band gap. As the depth increases, the indium content decreases.

The PL method was used to obtain the band gap of the surface of different CIGS films. Figure 2 shows the photoluminescence spectrum measured by PL. When GGI is 1.00, the film is $CuGaSe_2$, and the band gap is 1.66 eV, which is consistent with the reported value [29]. With the increase in indium content, the surface band gap gradually decreases. The values of the band gaps are 1.59 eV, 1.55 eV, and 1.48 eV, when GGI are 0.90, 0.81, and 0.72, respectively. Table 2 shows the surface GGI measured by ICP-OES and the band gaps calculated by Equation (1). The band gaps of the surface are slightly higher than that calculated from ICP. In the preparation of CIGS by selenization after sputtering, Ga is easy to enrich on the back surface, result in a lower GGI at the surface, leading to a decrease in the open circuit voltage [36]. For the CuIn/CuGa precursor in this work, after annealing the band gap of the surface is higher than that of the average, which is helpful for the improvement of the open circuit voltage.

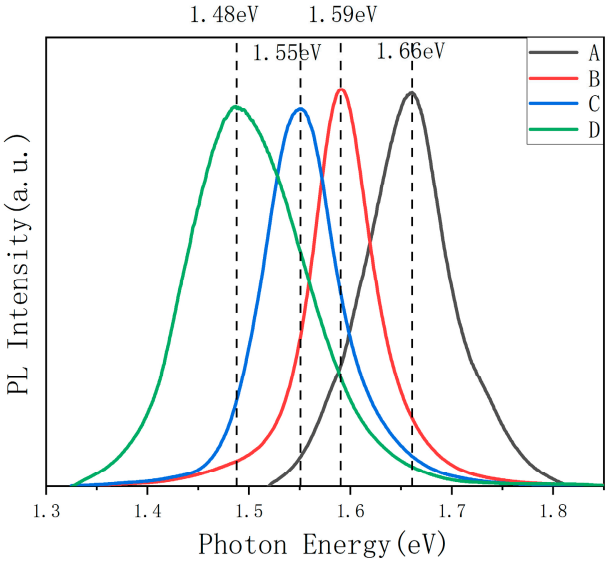

Figure 2. The PL spectra of the CIGS films with different gallium content.

Table 2. The Ga/(In+Ga) measured by ICP and the band gap measured by PL.

	Sample A	Sample B	Sample C	Sample D
Ga/(In+Ga) measured by ICP	1.00	0.90	0.81	0.72
Calculated E_g(eV)	1.66	1.59	1.52	1.45
E_g measured by PL (eV)	1.66	1.59	1.55	1.48

The XRD pattern and lattice constants of a and c are shown in Figure 3. All samples show good crystallinities, and the grains mainly grow along (1 1 2) direction. The diffraction peaks at 2θ of near 27.77°, 45.74°, 46.23°, 54.33°, and 55.15° correspond to the (1 1 2), (2 2 0), (2 0 4), (3 1 2), and (1 1 6) planes of CGS phase (# 75-0104), respectively. The (2 2 0) and (2 0 4) reflections are split at the room temperature, which is due to the tetragonal distortion in CIGS [37]. With the increase in Ga content, the peak position gradually shifts to the right, and the strength of the high angle (2 0 4) peak gradually increases. When Ga

completely replaces In, the peak strength of the (2 0 4) peak increases significantly. This is because the atomic radius of Ga is smaller than In. When Ga^{3+} replaces In^{3+}, the lattice size decreases [24]. The estimated lattice constants a and c in a unit of CIGS crystal were increased from 5.603 Å and 10.974 Å to 5.655 Å and 11.109 Å, respectively, with a decreasing GGI ratio from 1 to 0.72. This is because with the decrease in GGI, more In^{3+} with a larger ionic radius of 0.8 Å replaced Ga^{3+} with that of 0.62 Å. The variation of a and c for CIGS with GGI from 0.7 to 1.0 can be expressed as the following equations:

$$a(x) = -0.188x + 5.787 \quad (2)$$

$$c(x) = -0.506x + 11.478 \quad (3)$$

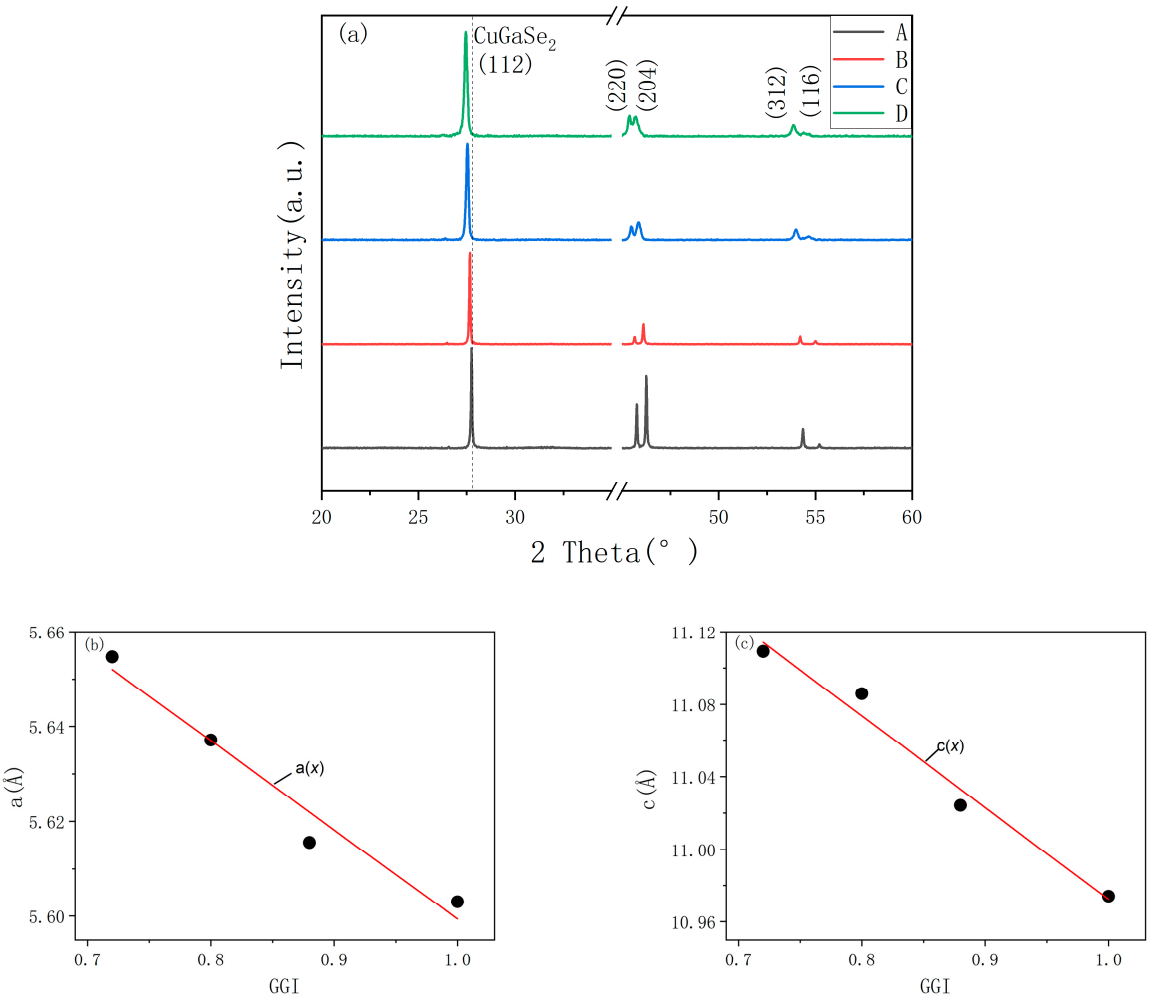

Figure 3. (**a**) The XRD spectra of the CIGS films with different gallium content, (**b**,**c**) lattice constants of a and c calculated from (**a**).

The peaks of (1 1 2) planes of Sample A to Sample D are 27.77°, 27.65°, 27.51°, and 27.46°, respectively. Combining with the (1 1 2) position of CuInSe2(26.67°, #80-0535), the GGI in the CIGS film can be calculated. For Sample B and Sample C, the ratios of Ga/(In+Ga) calculated by XRD are 0.88 and 0.80, respectively, which are smaller than the results detected by ICP. It is might due to a part of Ga atoms do not enter the crystal phase [33]. For Sample D, the ratio of Ga/(In+Ga) calculated by XRD is 0.72, which is equal to the result detected by ICP, it means that almost all of Ga atoms enter the crystal phase.

3.1.2. Characterization of CIGS Solar Cells

The solar cell J-V curve of CIGS cells using CdS as buffer layer is shown in Figure 4a. With the increase in indium content, solar cell efficiency gradually increases. Table 3 lists the performance parameters of different samples. When GGI is 0.72, the efficiency of the solar cell achieves the highest value of 11.58%. With the increase in GGI, the band gap of the absorption layer increases, which decreases the spectral response range, and the short circuit current of the cell decreases significantly. When GGI is 0.72, the highest value of Jsc is 25.2 mA/cm^2. When GGI is 0.81, the open circuit voltage reaches the highest value. This is because when GGI is 1.00 and 0.90, a layer of high Ga content and poor Se content is formed at the Mo/CIGS surface. At the same time, a thin fault appears between this layer and CIGS layer, which intensifies the carrier recombination at the fault and affects the open circuit voltage, resulting in a high deficit of Voc. With GGI continuing to decrease, the layer at Mo/CIGS surface is replaced by CIGS grains and the fault disappears. Therefore, the open circuit voltage returns to the normal level, and decreases with the decrease in the surface band gap. The open circuit voltage reaches the highest value of 757 mV when GGI is 0.81. With the increase in GGI, the band gap of CIGS increases, which is mainly reflected in the increase in conduction band minimum (CBM) [19]. When GGI = 1.00, a "cliff like" is formed between the absorption layer CGS and the buffer layer CdS, which intensifies the carrier recombination at the CGS/CdS surface and reduces Voc and FF [38,39]. When GGI increases, the conduction band offset (CBO) between CIGS and CdS increases, so the filling factor decreases with the increase in GGI. Larsson F et al. used ZTO as the buffer layer and gained a CGS solar cell with high Voc of 1017 mV, which was much higher than CdS buffer (768 mV). Additionally, FF increased from 58.6% to 68.0% [24]. Therefore, changing a suitable buff layer should be considered in future work.

Figure 4 shows (b) the EQE curve of solar cells with different GGI, (c) the minimum band gap obtained from the EQE curve. Table 4 shows the comparison between surface band gap and minimum band gap in the CIGS absorbers. Among all absorbers with different GGI, the minimum band gap in the absorbers is smaller than the surface band gap.

Table 3. Performance parameters of CIGS solar cells.

Sample	Ga/(In+Ga)	Efficiency (%)	Voc (mV)	Jsc (mA/cm^2)	FF (%)	Voc,def (mV)
A	1.00	3.26	659	10.5	46.86	1001
B	0.90	4.76	610	14.8	52.70	980
C	0.81	7.79	758	18.6	55.20	792
D	0.72	11.58	702	25.2	65.55	778

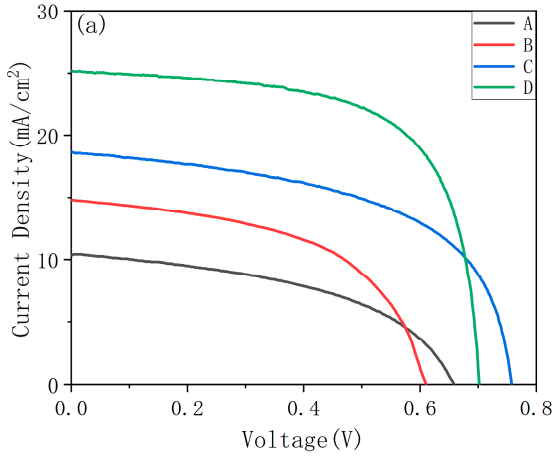

Figure 4. *Cont.*

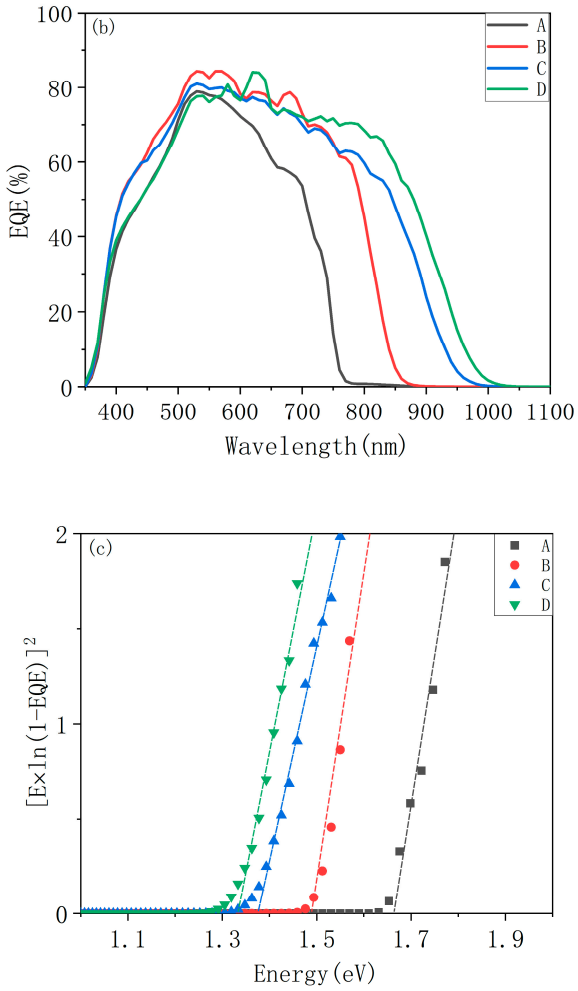

Figure 4. (**a**) The J-V curve of CIGS cells using CdS as buffer layer, (**b**) their corresponding EQE spectra, and (**c**) the minimum band gap obtained from the EQE curve.

Table 4. The band gap of CIGS measured by EQE and PL.

Sample	Eg_{min} (eV)	Eg by PL (eV)
A	1.66	1.66
B	1.49	1.59
C	1.37	1.55
D	1.34	1.48

According to the results of EDS, PL, and EQE, the Eg depth profile of CIGS absorbers can be obtained. The sketch of band gap of the CIGS absorber is shown in Figure 5. At the surface, the band gaps were measured by PL, the band gaps of Sample B, Sample C, and Sample D are 1.59 eV, 1.55 eV, and 1.48 eV, respectively, the indium content increases with depth. At the depth of about 300 nm, indium content reaches the maximum value. Meanwhile, the CIGS film has a minimum band gap which was measured by EQE. The values are 1.49 eV, 1.37 eV, 1.34 eV, respectively. As shown in Figure 1, with the depth continuing to increase, the indium content begins to decrease, causing the increase in GGI, the band gap increases. The band gap of CIGS film presents like a V-shaped. A wider band gap at the surface makes the solar cell obtain a high open-circuit voltage; additionally, a lower band gap minimum makes the solar cell have a high short-circuit current [40].

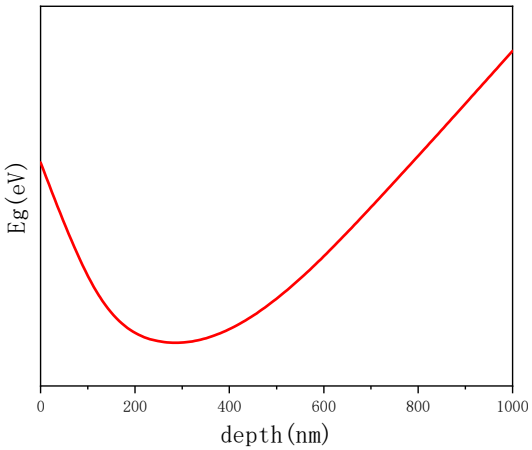

Figure 5. The sketch of Eg depth profile of CIGS absorber.

4. Conclusions

The properties of $CuInGaSe_2$ thin films and solar cells with different Ga contents were investigated. The results showed that using the structure of CuIn/CuGa as a precursor, a double-graded band gap profile can be obtained after selenidation annealing, which can make the solar cell have high open circuit voltage and high short circuit current. With the decrease in GGI, the solar cell efficiency increases gradually. The highest efficiency obtained in this work is 11.58% at GGI of 0.72. When GGI is 0.81, the maximum open circuit voltage of 757 mV obtained. CIGS solar cells with wide band gap show the potential to be suitable materials for top cells of CIGS tandem solar cells.

Author Contributions: Conceptualization, X.L. and Z.Z.; methodology, X.L. and Z.Z.; validation, X.L., Z.Z., and H.W.; formal analysis, X.L and H.W; resources, D.Z. and M.Z.; writing—original draft preparation, X.L.; writing—review and editing, D.Z and M.Z. All authors have read and agreed to the published version of the manuscript.

Funding: This work was supported by National Natural Science Foundation of China (NSFC, Grants 61974008).

Data Availability Statement: Any further details relevant to this study may be obtained from the authors upon a reasonable request.

Conflicts of Interest: The authors declare no conflict of interest.

References

1. Zeenat; Maryum Javed, S.; Ahmad, Z.; Ahmed, S.; Iqbal, S.; Naqvi, I.J.; Usman, M.; Ashiq, M.N.; Elnaggar, A.Y.; El-Bahy, Z.M. Highly dispersed active sites of Ni nanoparticles onto hierarchical reduced graphene oxide architecture towards efficient water oxidation. *Fuel* **2022**, *312*, 122926. [CrossRef]
2. Kuang, C.; Tan, P.; Javed, M.; Humaira Khushi, H.; Nadeem, S.; Iqbal, S.; Alshammari, F.H.; Alqahtani, M.D.; Alsaab, H.O.; Awwad, N.S.; et al. Boosting photocatalytic interaction of sulphur doped reduced graphene oxide-based S@rGO/NiS_2 nanocomposite for destruction of pathogens and organic pollutant degradation caused by visible light. *Inorg. Chem. Commun.* **2022**, *141*, 109575. [CrossRef]
3. Li, H.; Ji, H.; Liu, J.; Liu, W.; Li, F.; Shen, Z. Interfacial modulation of $ZnIn_2S_4$ with high active Zr-S_4 sites for boosting photocatalytic activation of oxygen and degradation of emerging contaminant. *Appl. Catal. B Environ.* **2023**, *328*, 122481. [CrossRef]
4. Kwok, K.C.S.; Hu, G. Wind energy system for buildings in an urban environment. *J. Wind. Eng. Ind. Aerodyn.* **2023**, *234*, 105349. [CrossRef]
5. Hussain, B.; Asif Ali Naqvi, S.; Anwar, S.; Usman, M. Effect of wind and solar energy production, and economic development on the environmental quality: Is this the solution to climate change? *Gondwana Res.* **2023**, *119*, 27–44. [CrossRef]
6. Li, L.; Li, M.; Qin, Y.; Chen, Y.; Dai, W.; Zhang, Z.; Kong, X.; Gong, P.; Wang, Y.; Yang, R.; et al. Eicosane-based thermo-conductive phase change composite for efficient capture solar energy and using in real-environment as power source. *Chem. Eng. J.* **2023**, *462*, 142273. [CrossRef]
7. Chandramohan, M.; Velumani, S.; Venkatachalam, T. Band structure calculations of $Cu(In_{1-x}Ga_x)Se_2$. *Mater. Sci. Eng. B* **2010**, *174*, 200–204. [CrossRef]

8. Nakamura, M.; Yamaguchi, K.; Kimoto, Y.; Yasaki, Y.; Kato, T.; Sugimoto, H. Cd-Free Cu(In,Ga)(Se,S)$_2$ Thin-Film Solar Cell with Record Efficiency of 23.35%. *IEEE J. Photovolt.* **2019**, *9*, 1863–1867. [CrossRef]
9. Hatt, T.; Schulze, P.S.C.; Er-Raji, O.; Richter, A.; Efinger, R.; Schultz-Wittmann, O.; Heydarian, M.; Tutsch, L.; Goldschmidt, J.C.; Glatthaar, M.; et al. Plated copper electrodes for two-terminal perovskite/silicon tandem solar cells. *Sol. Energy Mater. Sol. Cells* **2022**, *246*, 111912. [CrossRef]
10. Chantana, J.; Takeguchi, K.; Mavlonov, A.; Kawano, Y.; Minemoto, T. Correlation between detailed balance limit and actual environmental factors for perovskite/crystalline Si tandem solar cells with different structures. *Mater. Sci. Semicond. Process.* **2022**, *152*, 107085. [CrossRef]
11. Luo, J.; Tang, L.; Wang, S.; Yan, H.; Wang, W.; Chi, Z.; Gong, J.; Li, J.; Xiao, X. Manipulating Ga growth profile enables all-flexible high-performance single-junction CIGS and 4 T perovskite/CIGS tandem solar cells. *Chem. Eng. J.* **2023**, *455*, 140960. [CrossRef]
12. Elbar, M.; Tobbeche, S.; Merazga, A. Effect of top-cell CGS thickness on the performance of CGS/CIGS tandem solar cell. *Sol. Energy* **2015**, *122*, 104–112. [CrossRef]
13. Saad, M.; Kassis, A. Current–voltage analysis of the record-efficiency $CuGaSe_2$ solar cell: Application of the current separation method and the interface recombination model. *Sol. Energy Mater. Sol. Cells* **2011**, *95*, 1927–1931. [CrossRef]
14. Bouanani, B.; Joti, A.; Bachir Bouiadjra, F.S.; Kadid, A. Band gap and thickness optimization for improvement of CIGS/CIGS tandem solar cells using Silvaco software. *Optik* **2020**, *204*, 164217. [CrossRef]
15. Elbar, M.; Tobbeche, S. Numerical Simulation of CGS/CIGS Single and Tandem Thin-film Solar Cells using the Silvaco-Atlas Software. *Energy Procedia* **2015**, *74*, 1220–1227. [CrossRef]
16. Schmid, M.; Caballero, R.; Klenk, R.; Krč, J.; Rissom, T.; Topi, M.; Lux-Steiner, M.C. Experimental verification of optically optimized $CuGaSe_2$ top cell for improving chalcopyrite tandems. *EPJ Photovolt.* **2010**, *1*, 10601.
17. Hedayati, M.; Olyaee, S.; Ghorashi, S.M.B. The Effect of Adsorbent Layer Thickness and Gallium Concentration on the Efficiency of a Dual-Junction Copper Indium Gallium Diselenide Solar Cell. *J. Electron. Mater.* **2019**, *49*, 1454–1461. [CrossRef]
18. Dos Santos, R.B.; Rivelino, R.; Mota Fde, B.; Kakanakova-Georgieva, A.; Gueorguiev, G.K. Feasibility of novel $(H_3C)_nX(SiH_3)_{3-n}$ compounds (X = B, Al, Ga, In): Structure, stability, reactivity, and Raman characterization from ab initio calculations. *Dalton Trans.* **2015**, *44*, 3356–3366. [CrossRef]
19. Chen, X.-D.; Chen, L.; Sun, Q.-Q.; Zhou, P.; Zhang, D.W. Hybrid density functional theory study of $Cu(In_{1-x}Ga_x)Se_2$ band structure for solar cell application. *AIP Adv.* **2014**, *4*, 087118. [CrossRef]
20. Wei, S.H.; Zunger, A. Band offsets and optical bowings of chalcopyrites and Zn-based II-VI alloys. *J. Appl. Phys.* **1995**, *78*, 3846–3856. [CrossRef]
21. Khelifi, S.; Brammertz, G.; Choubrac, L.; Batuk, M.; Yang, S.; Meuris, M.; Barreau, N.; Hadermann, J.; Vrielinck, H.; Poelman, D.; et al. The path towards efficient wide band gap thin-film kesterite solar cells with transparent back contact for viable tandem application. *Sol. Energy Mater. Sol. Cells* **2021**, *219*, 110824. [CrossRef]
22. Kawano, Y.; Chantana, J.; Nishimura, T.; Mavlonov, A.; Minemoto, T. [Ga]/([Ga]+[In]) profile controlled through Ga flux for performance improvement of Cu(In,Ga)Se_2 solar cells on flexible stainless steel substrates. *J. Alloys Compd.* **2022**, *899*, 163276. [CrossRef]
23. Tu, L.-H.; Cai, C.-H.; Lai, C.-H. Tuning Ga Grading in Selenized Cu(In,Ga)Se_2 Solar Cells by Formation of Ordered Vacancy Compound. *Solar RRL* **2020**, *5*, 2000626. [CrossRef]
24. Larsson, F.; Nilsson, N.S.; Keller, J.; Frisk, C.; Kosyak, V.; Edoff, M.; Törndahl, T. Record 1.0 V open-circuit voltage in wide band gap chalcopyrite solar cells. *Prog. Photovolt. Res. Appl.* **2017**, *25*, 755–763. [CrossRef]
25. Eisenbarth, T.; Unold, T.; Caballero, R.; Kaufmann, C.A.; Abou-Ras, D.; Schock, H.W. Origin of defects in $CuIn_{1-x}Ga_xSe_2$ solar cells with varied Ga content. *Thin Solid Film.* **2009**, *517*, 2244–2247. [CrossRef]
26. Steichen, M.; Larsen, J.; Gütay, L.; Siebentritt, S.; Dale, P.J. Preparation of $CuGaSe_2$ absorber layers for thin film solar cells by annealing of efficiently electrodeposited Cu–Ga precursor layers from ionic liquids. *Thin Solid Film.* **2011**, *519*, 7254–7258. [CrossRef]
27. Popp, A.; Pettenkofer, C. Epitaxial growth of $CuGaSe_2$ thin-films by MBE—Influence of the Cu/Ga ratio. *Appl. Surf. Sci.* **2017**, *416*, 815–823. [CrossRef]
28. Jung, S.; Kim, J. Growth and Structural Characteristics of $CuGaSe_2$ Films Fabricated from Metallic Precursors Followed by an Elemental Se Reaction Process. *J. Nanosci. Nanotechnol.* **2016**, *16*, 5279–5284. [CrossRef]
29. Wei, Y.; Zhuang, D.; Zhao, M.; Zhang, N.; Yu, X.; Sun, R.; Zhang, L.; Lyu, X.; Peng, X.; Wei, J. Fabrication of wide band-gap $CuGaSe_2$ solar cells for tandem device applications by sputtering from a ternary target and post selenization treatment. *Mater. Lett.* **2018**, *230*, 128–131. [CrossRef]
30. Zhuk, S.; Kushwaha, A.; Wong, T.K.S.; Masudy-Panah, S.; Smirnov, A.; Dalapati, G.K. Critical review on sputter-deposited Cu_2ZnSnS_4 (CZTS) based thin film photovoltaic technology focusing on device architecture and absorber quality on the solar cells performance. *Sol. Energy Mater. Sol. Cells* **2017**, *171*, 239–252. [CrossRef]
31. Ramanujam, J.; Singh, U.P. Copper indium gallium selenide based solar cells—A review. *Energy Environ. Sci.* **2017**, *10*, 1306–1319. [CrossRef]
32. Peng, X.; Zhao, M.; Zhuang, D.; Guo, L.; Ouyang, L.; Sun, R.; Zhang, L.; Wei, Y.; Zhan, S.; Lv, X.; et al. Multi-layer strategy to enhance the grain size of CIGS thin film fabricating by single quaternary CIGS target. *J. Alloy. Compd.* **2017**, *710*, 172–176. [CrossRef]

33. Wang, C.; Zhuang, D.; Zhao, M.; Wei, Y.; Lyu, X.; Ren, G.; Wu, Y.; Hu, L.; Li, Y.; Gong, Q.; et al. The effects of preheating temperature on $CuInGaSe_2$/CdS interface and the device performances. *Sol. Energy* **2019**, *194*, 11–17. [CrossRef]
34. Ider, M.; Pankajavalli, R.; Zhuang, W.; Shen, J.Y.; Anderson, T.J. Thermochemistry of the Cu_2Se–In_2Se_3 system. *J. Alloy. Compd.* **2014**, *604*, 363–372. [CrossRef]
35. Ider, M.; Pankajavalli, R.; Zhuang, W.; Shen, J.Y.; Anderson, T.J. Thermochemistry of the Ga-Se System. *ECS J. Solid State Sci. Technol.* **2015**, *4*, Q51–Q60. [CrossRef]
36. Liang, H.; Avachat, U.; Liu, W.; van Duren, J.; Le, M. CIGS formation by high temperature selenization of metal precursors in H_2Se atmosphere. *Solid-State Electron.* **2012**, *76*, 95–100. [CrossRef]
37. Aninat, R.; van den Bruele, F.J.; Schermer, J.J.; Tinnemans, P.; Emmelkamp, J.; Vlieg, E.; van der Vleuten, M.; Linden, H.; Theelen, M. In-situ XRD study on the selenisation parameters driving Ga/In interdiffusion in Cu(In,Ga)Se_2 in a versatile, industrially-relevant selenisation furnace. *Sol. Energy* **2021**, *230*, 1085–1094. [CrossRef]
38. Minemoto, T.; Matsui, T.; Takakura, H.; Hamakawa, Y.; Negami, T.; Hashimoto, Y.; Uenoyama, T.; Kitagawa, M. Theoretical analysis of the effect of conduction band offset of window/CIS layers on performance of CIS solar cells using device simulation. *Sol. Energy Mater. Sol. Cells* **2001**, *67*, 83–88. [CrossRef]
39. Sobayel, M.K.; Chowdhury, M.S.; Hossain, T.; Alkhammash, H.I.; Islam, S.; Shahiduzzaman, M.; Akhtaruzzaman, M.; Techato, K.; Rashid, M.J. Efficiency enhancement of CIGS solar cell by cubic silicon carbide as prospective buffer layer. *Sol. Energy* **2021**, *224*, 271–278. [CrossRef]
40. Zhang, Y.; Lin, S.; Hu, Z.; Cheng, S.; He, Z.; Zhou, Z.; Sun, S.; Liu, W.; Sun, Y. Towards an optimized gallium gradient for Cu(In,Ga)Se_2 thin film via an improved constant low-temperature deposition process. *Sol. Energy Mater. Sol. Cells* **2020**, *209*, 110425. [CrossRef]

Disclaimer/Publisher's Note: The statements, opinions and data contained in all publications are solely those of the individual author(s) and contributor(s) and not of MDPI and/or the editor(s). MDPI and/or the editor(s) disclaim responsibility for any injury to people or property resulting from any ideas, methods, instructions or products referred to in the content.